JOURNAL OF AIRCRAFT
Vol. 43, No. 6, November–December 2006

Cooperative Control of Multiple Unmanned Aerial Vehicles Using the Potential Field Theory

Yeonju Eun* and Hyochoong Bang†
Korea Advanced Institute of Science and Technology, Daejon 305-701, Republic of Korea

DOI: 10.2514/1.20345

A hierarchical and automated control strategy applicable to the typical suppression of enemy air defense missions that involve multiple unmanned aerial vehicles is addressed. The new path finding and planning method is based upon the potential field theory, whereas conventional approaches largely rely on the so-called Voronoi diagram. The potential field approach that has been widely used for robot path planning is modified into the suppression of enemy air defense maneuver satisfying various mission objectives. In particular, cooperative maneuvers of unmanned aerial vehicles to attack a common target are dealt with successfully by the proposed potential field approach. A simultaneous arrival condition from different departure points is satisfied by seeking a different set of candidate solutions for the given potential field. Despite increased numerical computational workload in the new method, it leads to significant advantages with smooth trajectory as illustrated by battlefield simulation results.

I. Introduction

COOPERATIVE control of multiple unmanned aerial vehicles (UAVs) and/or unmanned combat aerial vehicles (UCAVs) has been an emerging issue for future applications to sophisticated military missions. In particular, various new concepts using UAVs for challenging missions are under active investigation. Path planning is a crucial step in establishing mission objectives before actual operation. It should take into account the given mission requirements as well as constraints imposed in performing the mission. Suppression of enemy air defense (SEAD) operation with multiple UAVs may be regarded as a primary future military tactic that requires well-established mission design tools such as path planning and trajectory generation capability.

As a typical battlefield scenario of a SEAD mission, let us consider a group of N UAVs required to deliver munitions on M known target locations. In addition, there are already known threats and unknown pop-up threats that may appear during operation as illustrated in Fig. 1. This scenario is well described in [1]. There are some requirements for the UAV systems to be tailored to the SEAD mission. The UAVs should be true air vehicles, more like manned aircraft rather than intelligent cruise missiles, to accomplish a variety of submissions, reconnaissance, or return-to-base operations. It should also be possible to fly the UAVs into the battlefield, and the cost is expected to be generally lower than manned air vehicles. Moreover, the most important requirement is that the entire process of the missions such as path finding and planning, detection of threats (for example, radars), assignment of each UAV to the targets, determination of feasibility of attack, and safe return-to-base in an infeasible attack condition has to be made fully automated. Thus the mission objectives can be achieved without intervention of human operation during the planning and operation. In Fig. 1, each target is assumed to be equipped with anti-aircraft measures, for instance, radars that detect the location of attacking aircraft, but these facilities are only capable of firing on one aircraft at a time.

Presented as Paper 6529 at the AIAA 3rd Unmanned Unlimited Technical Conference, Workshop and Exhibit, Chicago, IL, 20–23 September 2004; received 3 October 2005; revision received 14 August 2006; accepted for publication 15 August 2006.

*Graduate Student, Ph.D. Candidate, Division of Aerospace Engineering, Department of Mechanical Engineering; yjeun@fdcl.kaist.ac.kr.

†Associate Professor, Division of Aerospace Engineering, Department of Mechanical Engineering; hcbang@fdcl.kaist.ac.kr. Senior Member AIAA.

To maximize the probability of mission success in such situations, some requirements for the control strategy need to be established. First, an efficient assignment of UAVs to each target location is necessary. In the second, an optimal path-planning strategy is required to avoid dangerous threat regions and to save fuel and time. Third, when all the UAVs from different locations gain access to one target, each UAV is required to arrive at the boundary of the target radar detection region simultaneously and enter the attack region through different boundary points. Moreover, those tactics should be implemented in real time, to cope with an accidental situation such as the appearance of unknown pop-up threats. For the first requirement, efficient target assignment, Beard and McLain [1] suggested a target management strategy using acceptability and rejectability functions for each target. For the second requirement of the optimal path, the Voronoi diagram and the so-called k-shortest path search algorithm have been discussed in previous papers [2–5]. Not only the shortest path but also the k-shortest paths should be found for rendezvous missions. The k-shortest paths of each UAV from the start point to the target constitute multiple candidate paths to satisfy the simultaneous arrival constraint. The searching algorithms for the k-shortest paths have been investigated in many papers [6,7]. But a general case of the k-shortest paths search problem is so complicated, thus still significant research effort is focused on this issue. Finally, for the third requirement, the decomposition strategy has been suggested in [4].

A majority of the methods introduced above take the candidate paths generated by the Voronoi-diagram approach. Robot path planning using the Voronoi diagram has been studied widely since the mid-1980s [8], and a cooperative path-planning study for multiple UAVs was started in the late 1990s. The Voronoi diagram is considered as one of the most efficient methods for the SEAD maneuver planning. It possesses many advantages but, at the same time, suffers from some disadvantages as well. For example, it is rather difficult to extend the path planning to a three-dimensional space with the Voronoi diagram, and it is highly inefficient when real obstacle avoidance is required. Because the paths consist of discrete edges of the Voronoi diagram, it is generally inappropriate for smooth trajectory generation tasks.

In this study, a new path-planning technique is proposed for a SEAD maneuver by multiple UAVs. The key idea is to use the potential field method that has been popular in the robot path-planning areas. The potential field approach is adapted to the SEAD mission to satisfy the given mission objectives. Disadvantages of the conventional Voronoi-diagram approach are partially resolved by the potential field-based path-planning method. But, the new method needs a relatively heavy computational load in the first stage of planning, but it is necessary only once before the UAVs initiate their

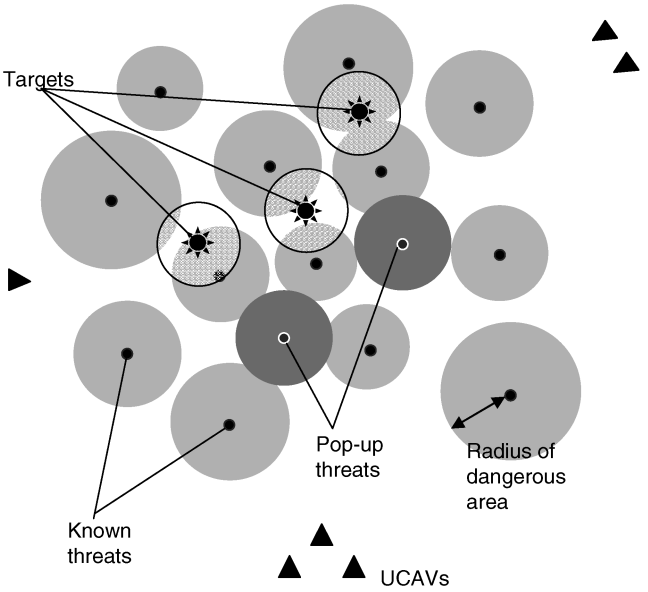

Fig. 1 Typical battlefield of SEAD mission.

missions. All the strategies introduced are required for target assignment and path planning, and thereby not iterative in nature. So, against accidental situations such as appearance of unknown threats or a certain UAV dropping out of the assigned group, reassignment and replanning should be achieved in real time. We investigate the path planning and strategies for a simultaneous attack which is usually performed after the assignment task.

This paper consists of four sections. In Secs. II and III, the new cooperative control scheme for the SEAD mission is described. Section II presents a modified potential field technique for path planning. In Sec. III, strategies for the SEAD mission such as simultaneous attack and dealing with pop-up threats are presented. The new proposed control strategy is compared with the conventional Voronoi-diagram approach through a simulation study in Sec. IV. Finally, the conclusion is presented in Sec. V.

II. Modified Potential Field Method for Path Planning

Path planning for the SEAD mission in this study is conceptually based on the mobile robot path-planning technique with obstacle avoidance. The Voronoi-diagram tool also has been applied to robot path planning since the mid-1980s. Path planning with simultaneous obstacle avoidance or motion planning of manipulators with collision avoidance has been an issue of utmost importance in robotics in recent years. It is a well-known problem, and many solutions have been suggested already.

The main research for solving the path-planning problems can be classified into global and local methods, respectively. The global method requires complete information of the environment since it is based on a global world representation and information. Different global methods have been investigated such as the grid of visit, numeric potential fields, graphs using the A* algorithm (graphs of visibility, of tangents, Voronoi), behavior-based models, genetic algorithms, and others [9]. In general, construction and maintenance of a global model involves heavy computational work as well as a large amount of memory resource [9].

On the other hand, the local path planners take only local information in a reactive manner. The local path planners are typically simpler than the global ones, because they can directly convert the sensor reading into actions. The next action is taken according to the local environment: potential field, the bug algorithm, behavior-based models, probabilistic models (virtual field histogram, occupancy grids), fuzzy logic, etc. [9]. Even if the local planners are simpler, they do not generally guarantee global convergence to the goal point.

For this reason, we can see that global path-planning methods are more appropriate than the local ones for the SEAD mission. Moreover, one has to provide several candidate paths for one UAV for the rendezvous at the goal location. Hence, the global path-planning methods are adopted in this study. And the potential field method is used to generate the initial paths. The path-planning technique using the artificial potential field and/or physical potential field has been investigated since the mid-1980s in various applications. An elegant approach for obstacle avoidance in $\mathbf{R}^n$ by the artificial potential field technique was pioneered by Khatib [10], followed by many others.

As mentioned earlier, the global path planning is more appropriate for the SEAD mission, and the artificial potential field method is employed for the path planning. This implies that a potential field should be constructed at each point in free space, that is, over the global space. The primary principle of the path planning with a global potential field is to construct a suitable potential field with an attractive global minimum at the goal point and repulsive local maxima at the obstacles. The path is then generated by following the gradient of a weighted sum of the potentials. A number of artificial potential functions have been proposed in past decades. In this study, we use the mass diffusion equation to construct the potential field [11]. The goal point (target point of the SEAD), G, is considered as the location of a virtual source with some gaseous material, for example, a scent or a perfume. With the concentration at point G kept constant, the material diffuses steadily into the neighboring space. As a result, the concentration distribution develops about both time and space. In the steady equilibrium state, the distribution tends to be a monotonously decreasing concentration along the path between the goal point, the point of maximum scent concentration, and an arbitrary starting point S within the space filled with the gaseous material. The path between S and G can be easily constructed by taking the steepest ascent strategy, that is, streamline generation using the potential field [11].

To make this approach amenable to the SEAD mission, first we define the dangerous area of each threat. The dangerous area is defined as a circle with its center at the threat location. It can be obtained from initially known information, the power level of radars, etc. In a real battlefield, the radar power level may not be identical. If the radar information is available, it will certainly improve the planning result. To make it different from other path-planning approaches, we define the region to be avoided in two sections: a critical area (very dangerous area), and a less dangerous area. The boundaries of the critical areas are treated as boundaries of the obstacles in the diffusion field. The mass concentration in this area is assigned a constant value, zero. Consequently, the path, or streamline cannot enter the critical areas ever in practice. Thus, the critical area should be specified as the most dangerous area being close to the threat. It may be too dangerous to pass the critical area, and the less dangerous areas are defined to be less dangerous than the critical area. The critical area and the dangerous area for one threat are concentric circles in general, and they could overlap each other as shown in Fig. 2.

Now, we attempt to solve the unsteady diffusion equation given by Eq. (1) with the boundary conditions and source at the goal position, G. Then we can construct the desired potential field based upon the solution. The boundary condition is characterized by a constant concentration as the initial value on the whole field, $u(0, x)$. An unsteady diffusion equation is given by [11]

$$\frac{\partial u}{\partial t} = a^2 \cdot \nabla^2 u - g \cdot u \tag{1}$$

where $u(t, \underline{x})$ is defined over the space and time, and the Laplace operator $\nabla^2 u$ is defined as

$$\nabla^2 u = \frac{\partial^2 u}{\partial x^2} + \frac{\partial^2 u}{\partial y^2} \tag{2}$$

The boundary conditions are prescribed as

$$u(t, \underline{x}_G) = 1000, \qquad \underline{x}_G \in \Omega \subset R^2, \qquad u(t, \underline{x}_0) = 0, \qquad \underline{x}_0 \in \delta\Omega \subset R^2 \tag{3}$$

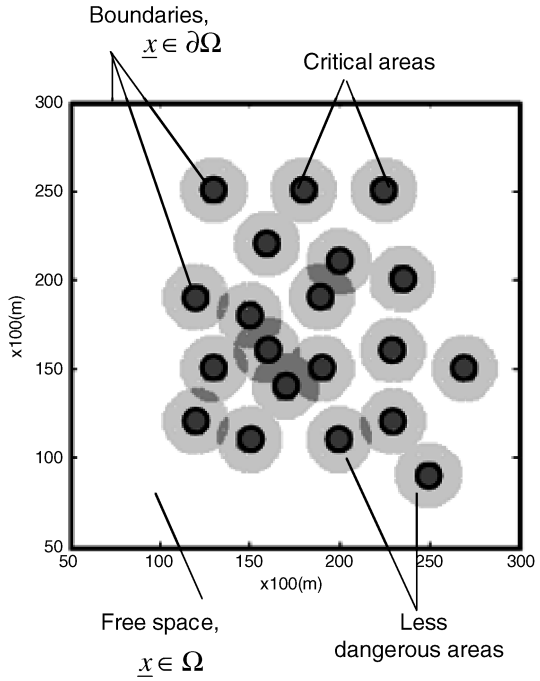

Fig. 2 Critical and dangerous areas and boundaries for the mass diffusion problem.

while the initial condition is set to be $u(0, \underline{x}) = 0$, for $\underline{x} \in \Omega \subset \mathbf{R}^2$. Also, $u(t, \underline{x})$ denotes the concentration function over time and the Cartesian space with $\underline{x} = [x, y]^T \in (\Omega \cup \delta\Omega) \subset \mathbf{R}^2$. Moreover, Ω is defined as a closed connected region, that is, the battlefield including the goal point, $\underline{x}_G$. The boundary set $\delta\Omega$ is formed by the obstacles and free space boundaries as shown in Fig. 2. In a physical sense, the concentration has to be zero at the initial time and at the boundaries of obstacles where the diffusion occurs all the time. Note that $u(t, \underline{x}_G)$ can have any arbitrary positive value, and it has to be determined just based upon resolution and/or computational efficiency. The constants a^2 and $g \geq 0$ represent the diffusion constant and the substance disintegration rate, respectively [11].

Solution of the diffusion equation can be obtained by analytical or numerical approaches. In general, the boundaries are too complicated to be solved analytically; hence in this study a numerical method, FDM (finite difference method) approach is employed. By application of the standard finite difference method, Eq. (4) as a discretized version of Eq. (2) over time and space can be derived for a grid point or node, $r = (x, y) \in (\Omega \cup \delta\Omega)$ [11].

$$\frac{u(i+1, r) - u(i, r)}{\tau} = \frac{a^2}{h^2} \cdot \sum_{\substack{k=1 \\ m \in N(r)}}^{M} [u(i, m_k) - u(i, r)] - g \cdot u(i, r) \quad (4)$$

where τ denotes the time step and h is the grid width. In addition, $N(r)$ and M represent the set and number of neighboring nodes for the approximation of the Laplace operator $\nabla^2(\cdot)$. For $g = 0$, the fastest convergence of the finite difference scheme is achieved by selecting $a^2 = h^2/(\tau \cdot M)$ [11].

For the simulation in Sec. V, the battlefield, assumed as a 25 km × 25 km square, is divided into 250 × 250 elements (with 100 m in resolution), and all the elements in the FDM are squares of the same size. If the field is divided into smaller elements, the more accurate results can be obtained. But, excessive computational load should be accommodated in proportion. This work is not for a real mass diffusion analysis, instead it is just designed to derive the potential field with similar characteristics as that of the mass diffusion in the real world. Then, it is not necessary to divide the whole field into very small elements. Furthermore, this work needs to be completed before the UAVs take off, and one can possibly make use of parallel computing algorithms for efficient generation of the planning results.

After the potential field is generated by the numerical method described above, a steepest ascent path following the gradient of $u(t_\infty, \underline{x})$, the steady state mass diffusion, from arbitrary starting points (except the critical area) to the goal point, can be computed. Each path never comes across the critical area, and it is continuous and smooth. Especially, since the critical area is treated as obstacles obstructing the mass diffusion, the paths should avoid the critical area in some distance. But, if the critical areas are large, the problem cannot be solved quickly, because the passages between the obstacles are so narrow that it takes a longer time for the gaseous material to diffuse from the source to the arbitrary start point. In another case, it cannot find a path for more than two critical areas contacting each other. To avoid such problems, we keep the critical areas small and push the path out of the less dangerous areas by applying the repulsive force described below.

When the path constructed by the steepest ascent technique enters the dangerous area, then the repulsive force from the threats can be applied. This repulsive force is modeled as Eq. (5)

$$F = k\{(x - x_t)^2 + (y - y_t)^2\}^2 \|\nabla u(t_\infty, \underline{x})\| \quad (5)$$

where $\underline{x} = [x, y]^T$ is the current position and (x_t, y_t) denotes the threat position with the dangerous area concerned. Note that $\{(x - x_t)^2 + (y - y_t)^2\}^2$ is the fourth power of the distance to the threats. Because the strength of the radar signature is proportional to $1/\text{dist}^4$, the parameter dist^4 represents the measure of how far it should be apart from the threat [9]. In addition, $\|\nabla u(t_\infty, \underline{x})\|$, the norm of the gradient at the point (x, y) corresponds to the magnitude of tendency to go through the original path. The gain $k \in (0, 1)$ has to be determined by considering such factors as $\{(x - x_t)^2 + (y - y_t)^2\}^2$ and $\|\nabla u(t_\infty, \underline{x})\|$. Empirically in our simulation study, when taken in the range $k \in (0, 0.5)$, a better performance was achieved.

The resultant force $\mathbf{F}$, as a combination of attractive and repulsive forces from the goal point and obstacles, respectively, is given by Eqs. (6–8):

$$\mathbf{F} = \mathbf{F}_a - \mathbf{F}_r \quad (6)$$

$$\text{Attractive force}: \mathbf{F}_a(\underline{x}) = \nabla u(t_\infty, \underline{x}) \quad (7)$$

$$\text{Repulsive force}: \mathbf{F}_r = k\|\underline{x} - \underline{x}_t\|^4 \|\nabla u(t_\infty, \underline{x})\| \cdot \frac{\underline{x} - \underline{x}_t}{\|\underline{x} - \underline{x}_t\|} \quad (8)$$

where Eq. (8) corresponds to the vector expression of Eq. (5). As mentioned before, tthe numerical technique is used to solve the diffusion equation in general. In this process, one can apply the repulsive force directly to the constructed potential field of mass diffusion. That is, the repulsive potential from an obstacle can be superposed upon the initial attractive potential constructed already such as

$$u_{\text{modified}}(\underline{x}) = u(t_\infty, \underline{x}) + k\|\underline{x} - \underline{x}_t\|^4 \|\nabla u(t_\infty, \underline{x})\| \cdot \frac{\underline{x} - \underline{x}_t}{\|\underline{x} - \underline{x}_t\|} \quad (9)$$

In Fig. 3, a dashed line denotes the original path constructed without the repulsive force whereas a solid line represents the modified path

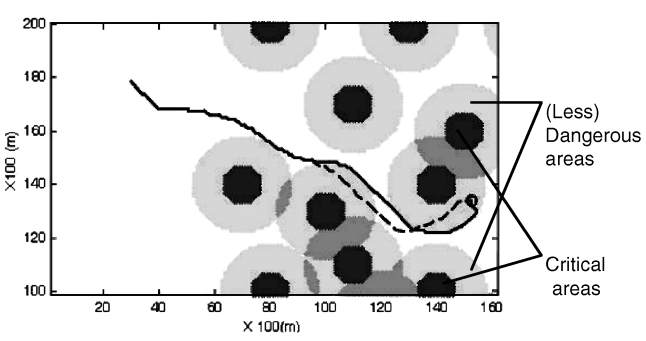

Fig. 3 Path modification using repulsive force.

generated with the repulsive force. As one can see, the modified path avoids the dangerous area by the repulsive force.

Repulsive force from the obstacles and attractive force from the goal point is a principal idea of the path planning using the artificial potential field. But the potential has to be evaluated at all points of the whole free space for the rendezvous at the goal. Hence, the special feature of this modified potential field method lies in that smaller critical area, where the path can never enter, determined for efficiency. The path is pushed out of the dangerous area by repulsive force if the path penetrates into the less dangerous areas. Consequently, the new method suggested in this section is made of a combination of both global and local path-planning approaches in conjunction with the artificial potential field.

III. Strategies for SEAD Mission

A. Strategies for a Simultaneous Attack

Up to now, construction of the potential field and associated path finding have been addressed. Each UAV has to be assigned more than one candidate path for simultaneous attack to fulfill the primary cooperative maneuver for the SEAD operation. But, through the potential field constructed, the path from a certain departure point to the goal point is uniquely generated. Thus, strategies to construct more candidate paths are needed, so that a final path out of multiple candidates satisfying the mission objectives can be selected. There are three strategies for this: the first strategy is to use the repulsive force, the second one is relying on the unsteady diffusion function, and the third strategy is a new potential filed construction with a sink at the start point. After construction of more candidate paths, a set of optimal paths that satisfy the minimum team cost are to be selected. For this procedure, first of all, each cost of the UAV should be clearly defined.

The total cost of each path will be evaluated by considering the path length and exposure as described below. Let $\underline{p}(t) = [x \quad y]^T(t) \in \mathbf{R}^2$ represent the position on the path at time t. Then, the costs are defined as follows:

$$\bar{J}_{\text{length}} = \int_0^{t_f} \|\dot{\underline{p}}(t)\| \, \mathrm{d}t, \qquad \bar{J}_{\text{exposure}} = \sum_{i=1}^{M} \int_0^{t_f} \frac{q_i}{\|\underline{p}(t) - \underline{x}_{t,i}\|^4} \, \mathrm{d}t \tag{10}$$

where M is the number of threats, $\underline{x}_{t,i}$ the position of the ith threat, and q_i represents the measure of danger from the radar power level of the ith threat. In the numerical method employed to solve the mass diffusion problem, $\underline{p}(t)$ can be discretized into the elements of FDM on the path. Let us consider $\underline{p}(t_j)$ as the position of the elements of FDM at time t_j and $\underline{p}(t_{j+1})$ of the next element on the same path. Because the distance between $\underline{p}(t_j)$ and $\underline{p}(t_{j+1})$ is relatively short and $t_{j+1} - t_j$ is small, for each segment $\overline{\underline{p}(t_j), \underline{p}(t_{j+1})}$, the costs can be approximated as follows:

$$\begin{aligned} \hat{J}_{\text{length},(j,j+1)} &= \|\underline{p}(t_j) - \underline{p}(t_{j+1})\|, \\ \hat{J}_{\text{exposure}(j,j+1)} &= \sum_{i=1}^{M} \int_{t_j}^{t_{j+1}} \frac{q_i}{\{\text{dist}(\underline{p}(\tau), \underline{x}_{t,i})\}^4} \, \mathrm{d}\tau \\ &= \sum_{i=1}^{M} \frac{q_i (t_{i+1} - t_i)}{\|1/2(\underline{p}(t_j) + \underline{p}(t_{j+1})) - \underline{x}_{t,i}\|^4} \end{aligned} \tag{11}$$

Sometimes, a normalized cost is convenient for the analysis overcoming a large difference between the length and the exposure costs. The normalized costs are formed as

$$\begin{aligned} J_{\text{length}_{(j,j+1)}} &= \frac{\hat{J}_{\text{length}_{(j,j+1)}} - \min(\hat{J}_{\text{length}_{(j,j+1)}})}{\max(\hat{J}_{\text{length}_{(j,j+1)}}) - \min(\hat{J}_{\text{length}_{(j,j+1)}})}, \\ J_{\text{exposure}_{(j,j+1)}} &= \frac{\hat{J}_{\text{exposure}_{(j,j+1)}} - \min(\hat{J}_{\text{exposure}_{(j,j+1)}})}{\max(\hat{J}_{\text{exposure}_{(j,j+1)}}) - \min(\hat{J}_{\text{exposure}_{(j,j+1)}})} \end{aligned} \tag{12}$$

Finally, the total cost consists of the two terms: the first term is the length cost and the second one is the exposure cost such that [2]

$$J = \sum_{j=1}^{N-1} J_{(j,j+1)}, \qquad J_{(j,j+1)} = \lambda J_{\text{length}_{(j,j+1)}} + (1 - \lambda) J_{\text{exposure}_{(j,j+1)}} \tag{13}$$

where $\lambda (0 \le \lambda \le 1)$ is a weighting factor for the length cost and J is the total cost of a complete path [2].

For the first strategy to construct multiple candidates, one can build up more than one path, for example, paths with and without the repulsive force. By incorporating the repulsive force, one can produce a safer candidate path, but it may result in a higher cost. Using the repulsive force, the threat exposure can be lowered, but the total cost as a combination of the threat exposure and length may not be lowered. The threat exposure cost is integrated by time, thus it will be difficult to handle when the total path length increases by the modified path. It is impossible to decide which one is better for the team level cost, so that both paths could be regarded as candidates.

Second, solving the unsteady diffusion equation allows us to construct additional paths. Because the unsteady diffusion equation is employed, one can get different potential fields at different time steps with just one iteration process. As a result of the diffusion process, there exists a minimum time delay before path computation from the start to the goal points is initiated. If the diffusion simulation is initiated at $i = 0$ in Eq. (4) with the initial function $u_{0;\underline{x}} = 0$, a minimum of $i = L$ time steps are required before diffusion reaches r_s, that is, $u_{L;r_z} \neq 0$, where L represents the number of grid nodes passed by the shortest path possible from the start S to the goal point G. For a fixed start and goal points, an average value for L can be computed from

$$L = c \cdot \sqrt[n]{n_g}, \qquad c = \text{const} \tag{14}$$

where n and n_g denote the dimension of space $\mathbf{R}^n$ ($n = 2$, for a planar case) and the total number of grid nodes, respectively [11]. Finally, we can construct some different paths from the potential field with all different concentration distributions due to the different time steps, i. Figure 4 shows two different paths from the same start point. The dotted line represents the path obtained from the potential field at the stage, $i = 5000$ while the solid line corresponds to $i = 10,000$.

If each UAV is assigned to the target to attack, members of a group attacking one target produce a similar cost. But it still does not guarantee the simultaneous arrival of the multiple UAVs to the given target. Thus further sophisticated trajectory planning strategy for each UAV is required. For coordinated control problems, the purpose of the decomposition is to break up a single, very large optimization problem into a set of smaller, more tractable optimization problems. This decomposition strategy has been developed in [3]. By using this decomposition strategy, one can determine the TOT (time over target [3]) of each team and each UAV assigned to the same target. Finally, a path satisfying the simultaneous arrival constraint can be constructed. In Fig. 4, it is assumed that the radar powers are all equal and the radii of dangerous areas are all the same also in order to

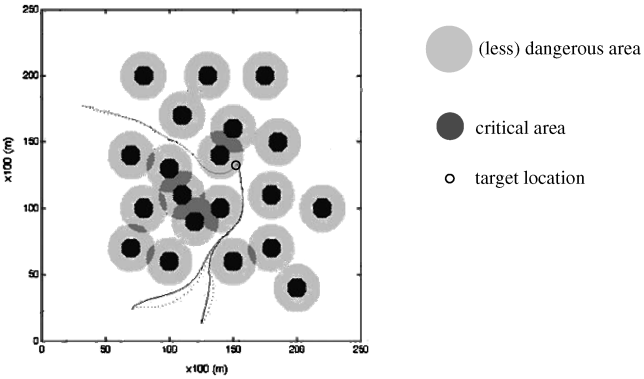

Fig. 4 Different paths by different time steps.

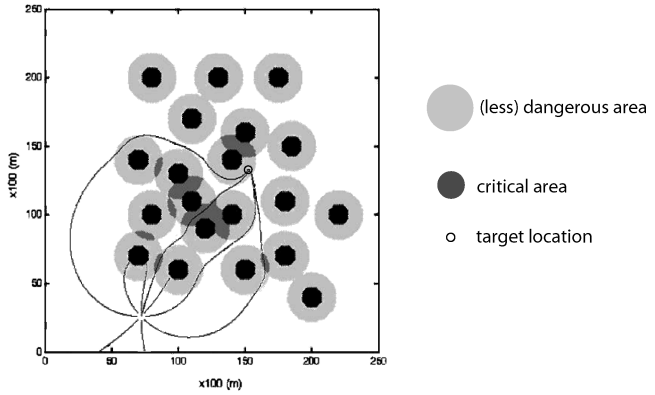

Fig. 5 Various paths with a sink at the start point.

compare with the simulation results of the Voronoi-diagram method under the same condition in Sec. V.

In the third strategy, different paths are generated from the new potential field constructed with a sink at the start point. Considering the start point as a sink such that $u(t, \underline{x}_s) = -10$, the new potential field is developed as a feasible candidate. The sink point is a strict singular point and it is impossible to start exactly from the sink point from the perspective of a numerical solution. Because of the problem of the exact starting point, a new starting point can be selected as a point on the arc of a circle that is a sufficiently small distance away from the sink. However, there exist many candidate paths associated with different initial directions around the circle as illustrated in Fig. 5. In Fig. 5, we can select the paths reaching the target as candidate ones. Because of the local maxima at the boundaries of critical areas, it is impossible for the two paths to reach the target location as shown in Fig. 5. These local maxima exist only in the potential field with a source at the goal point (target location) and a sink at the start point. And any negative value of $u(t, \underline{x}_s)$ is available at the start point. But, a too large negative value is liable to cause more candidate paths not to reach the goal point. With a too large negative value at the start point, a steeper slope in the solution trajectory can result, and the boundaries of the more critical areas with a constant boundary condition such as $u(t, \underline{x}_0) = 0, \underline{x}_0 \in \delta\Omega \subset \mathbf{R}^2$ would experience local maxima. Thus, it has to be determined based upon the distance among the start point, the nearest critical areas, and the goal position.

After the set of candidate paths for each UAV are generated, the length and threat exposure costs should be computed. Then the most appropriate path for each UAV is picked up for the purpose of simultaneous attack by the same decomposition strategy described in [3].

B. Strategies Against Pop-Up Threats

Each UAV is assumed to be equipped with sensors detecting radar signals, and all information about the pop-up threats is shared by all UAVs on the team in case one of them detects the pop-up threats in near real time. Then, a counterplan should be established against the unknown pop-up threats that may appear during the flight. The less dangerous area can be also determined as a circle with a radius as the distance between the current position and the pop-up threats. The critical area can be characterized after computation of hardware constants of the radars. The amount of power received by the radars is a function of the distance [12], and one can evaluate the radar power and the critical area as the UAVs navigate along the initial path. At this time, if each initial path of the UAVs does not enter the dangerous area, replanning is unnecessary, otherwise all the paths should be replanned. The replanning comprises two cases according to the current condition of each UAV; in the first case, the initial path is affected by the pop-up threats whereas it is unaffected in the other case.

First, the case for pop-up threats affecting the initial path is considered. The potential field that has been computed already does not reflect the presence of the pop-up threats. Thus, a strategy in the following is proposed to build some new candidate paths considering the pop-up threats.

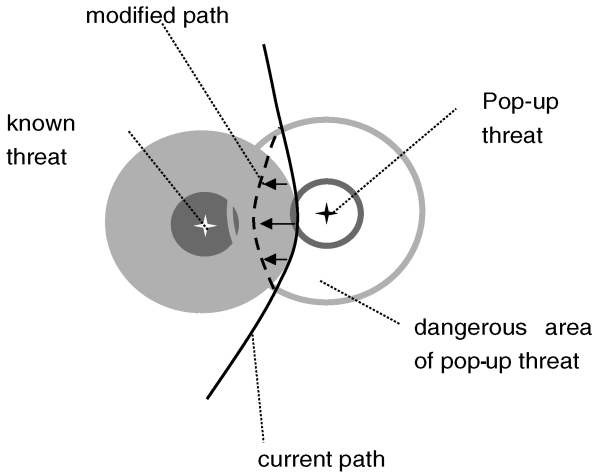

Fig. 6 Path modification against the pop-up threat.

1. *Modification of the Current Path*

In this approach, we modify only the section overlapping the dangerous area of the pop-up threats in the current path as illustrated in Fig. 6. The main principle is to employ a chain of mass system subject to virtual force from threats [2,13]. The initial path is divided into n sections of the same size, and each node is treated as a mass. These masses are connected in a single line, and spring-damper systems exist between masses. We call this system a chained mass system. Each mass is experiencing not only the force by the spring-damper systems, but also virtual repulsive force due to threats. The virtual force is created from the threats in their own dangerous areas where the masses exist. The direction of the virtual force is opposite to the vector from a mass to the threats. And magnitude of the virtual force depends on the priority of the threats determined by the radar power. The priority of danger of the pop-up threats may be higher than the original, in order to make them effective for path modification. This is because it does not affect the initial potential field and generated path as well. The start and end nodes are assumed as boundary conditions at fixed locations. For example, one of the equations of motion for each mass m_j is given as Eq. (15) [13]:

$$m_j \ddot{\underline{x}}_j = \underbrace{k(\underline{x}_{j-1} - \underline{x}_j) - k(\underline{x}_{j+1} - \underline{x}_j)}_{\text{spring forces}} + \underbrace{b(\dot{\underline{x}}_{j-1} - \dot{\underline{x}}_j) - b(\dot{\underline{x}}_{j+1} - \dot{\underline{x}}_j)}_{\text{damping forces}} + \underbrace{\sum_{i=1}^{M'} \frac{q_i(\underline{x}_j - \underline{x}_{t,i})}{|\underline{x}_j - \underline{x}_{t,i}|^5}}_{\text{virtual forces}} \tag{15}$$

$\underline{x}_j, \underline{x}_i \in \mathbf{R}^2$ in 2-D space or $\underline{x}_j, \underline{x}_i \in \mathbf{R}^3$ in 3-D space, where $\underline{x}_j$ denotes the position of mass m_j and $\underline{x}_{t,i}$ denotes the position of the ith threat. Moreover, M' represents the number of threats in their own dangerous areas where the mass m_j exists. The design parameters k and b correspond to spring constant and damping coefficient, respectively. Then, when we solve the dynamic equations of the chained mass system, a modified path can be designed as described in [2,13].

2. *Suitable Path Finding and Modification*

This strategy seeks to construct paths avoiding the pop-up threats while approaching the goal point. First of all, it is necessary to find the point A as a local goal point in Fig. 7 at a distance determined on the initial path. The global goal point can be a local goal point when the distance between the current and the global local point is shorter than the value determined. Then one has to build up some paths for the local goal point while avoiding the dangerous area of the pop-up threats. These paths can be found by examination through the

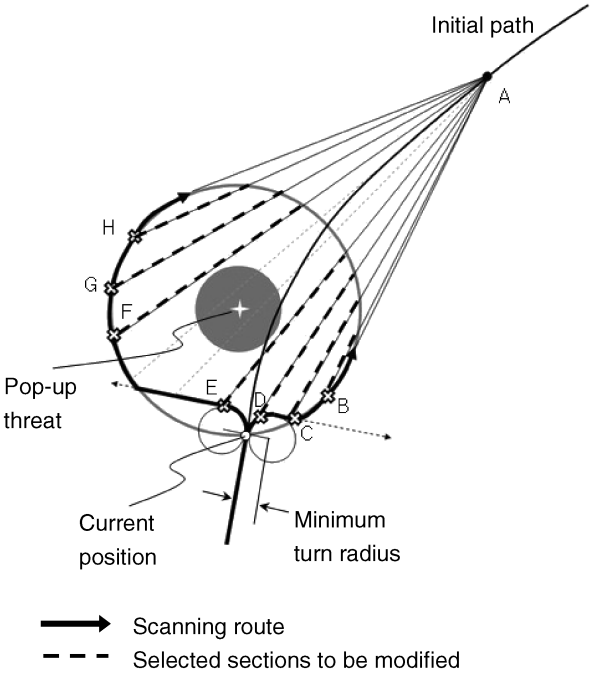

Fig. 7 Suitable path finding and modification.

scanning route. This scanning route is determined as follows: it turns to the left and the right with a minimum turn radius at the current position and moves forward to escape the dangerous area. After escaping the dangerous area, it follows along the boundary of the dangerous area. If this scanning route encounters the critical area of different threats, it stops at that point. In 3-D space, this scanning route consists of the intersection curve of the spherical dangerous area and the plane containing the current position and the local goal point, *A*.

Now we can choose different points where an appropriate path is initiated. For convenience, let the straight line connecting the arbitrary point to the local goal point be the LOS (line of sight) of the point. On the scanning route, some points whose LOSs do not overlap with the critical area such as points *B* to *H* in Fig. 7 can be selected by examining the LOSs. Consequently, each LOS overlapped with the dangerous area is selected and modified by the identical approach in the previous subsection. The scanning route can connect the current position to the modified path, and the paths just escaping the dangerous area can be constructed. Now a path to the global goal point should be established. This path is easily designed by using the potential field that has been discussed already in the initial planning stage.

Next, new paths of the UAV that will fly through the dangerous area by the pop-up threats can be constructed. Then one should find some candidate paths of other UAVs for the TOT* matching [1] condition. Using the unsteady diffusion equation, it is possible to construct the potential field again with a sink point at the current position of each UAV. Initial values are given as those of the potential field computed already. It makes sense that a sink suddenly appears during the unsteady diffusion. And at this time the minimum time step for numerical computation *L* in Eq. (9) should be indeed small due to the shortened distance to the goal point.

IV. Simulation Results

In this section, a simulation study for a sample SEAD scenario is presented. For a reasonable simulation study being close to real flight situations, the real-time trajectory generation has to be implemented. For several reasons, many physical restrictions are imposed on the trajectory generation of an aircraft, especially a fixed-wing aircraft. Recently, there is growing interest in the trajectory generation problems for a special class called "differentially flat systems" [14], and this concept was used in [1]. But using this method, we must solve the real-time optimization problem to satisfy all the given constraints. The real-time trajectory generation problem which is adoptable for an aircraft still remains to be studied. In our study, the method of differentially flat systems is used, and it shows satisfying results under not so tough conditions. For the mission conditions of three UAVs departing from different sites, one target and 20 known threats with their positions are given initially. And there exists an unknown pop-up threat also.

A. Simulation Results in the Case of Only Initially Known Threats

As the first step, the typical Voronoi node and edges are constructed by using the construction algorithm for the Voronoi diagram in [15]. For the next step, using the strategies described in [2–4], the best path set that satisfies simultaneous arrival at the target is determined as Fig. 8. For the real-time trajectory generation, the method of differentially flat systems [14] is adopted.

Figure 9a displays dangerous areas for the potential field methodology. As discussed already, it is assumed that the radar powers are all equal, and the radii of the dangerous area are also all the same for comparison with the simulation results by the Voronoi-diagram approach. After construction of the potential field, some candidate paths for each UAV are generated as Fig. 9b. Using the strategy for the TOT* matching and simultaneous attack, the best path set is determined such as Fig. 9c. Thus, this is a result of the initial path planning. In the TOT* matching strategy, the weighting factor λ of Eq. (3) is identical to that of the TOT* matching of the Voronoi-diagram method. Accordingly, a similar path set is selected in relation to the Voronoi-diagram case. TOT* is determined as

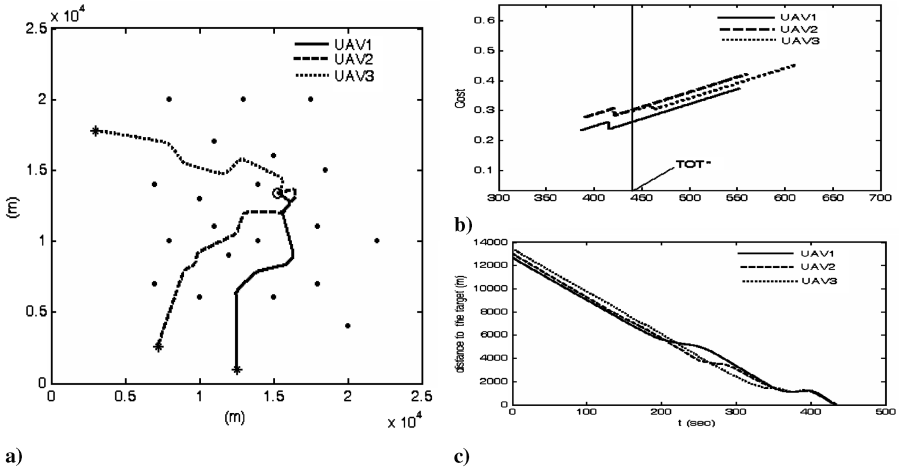

Fig. 8 Path-planning result without pop-up threats (using the Voronoi diagram). a) Trajectory generation result; b) coordinated variable of each UAV and TOT* matching; c) time vs distance to the target.

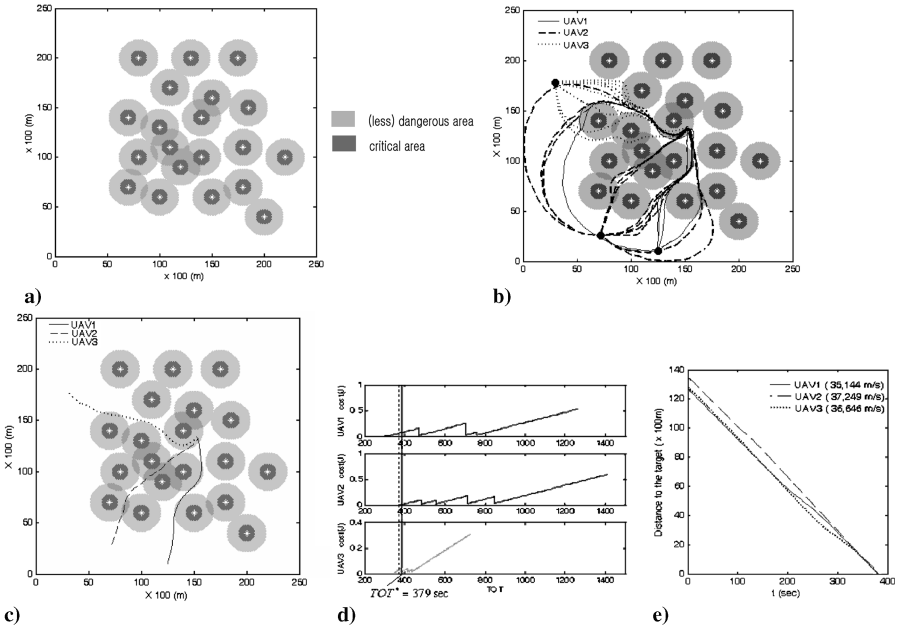

Fig. 9 Path-planning result without pop-up threats (using the potential field method). a) Dangerous areas of the virtual battlefield; b) candidate paths; c) trajectory generation result; d) coordinated variable of each UAV and TOT* matching; e) time vs distance to the target.

379 s, being shorter than TOT* (=408 s) of the Voronoi method. And one can observe also the path length is shorter than that of the Voronoi approach.

B. Simulation Results in the Case of Unknown Pop-Up Threat

Figures 10 and 11 illustrate results of the replanning case by the Voronoi and potential field approaches, respectively. It was assumed that all of the UAVs engaged in this mission can detect the pop-up threats in the range of 1500 m, and if one UAV detects a pop-up threat, then information of the pop-up threat is shared by other UAVs. As shown in Fig. 10a, during the mission operation, the UAV [1] (displayed with solid line) detects a pop-up threat. In Fig. 10b, the thin dashed line is a Voronoi diagram of initial condition and each UAV regenerates the Voronoi diagram and replans the path. Similarly, in Fig. 11a the UAV_1 detects the pop-up threat and each UAV computes its own candidate paths against the pop-up threat. Like the initial path-planning result, the best appropriate path set is determined as shown in Fig. 11b.

C. Analysis

From the simulation study, advantages of the new path planning compared to the Voronoi-diagram method can be summarized as follows:

1) As in the simulation results, the new approach shortens the unnecessarily elongated path length and results in a small TOT*. As discussed already, the threat exposure cost is integrated by time. This implies if a UAV is exposed to a weak threat for a long period of time, then the cost could be larger than that of the exposure to a strong threat for a short duration. Consequently, maintaining a small TOT*

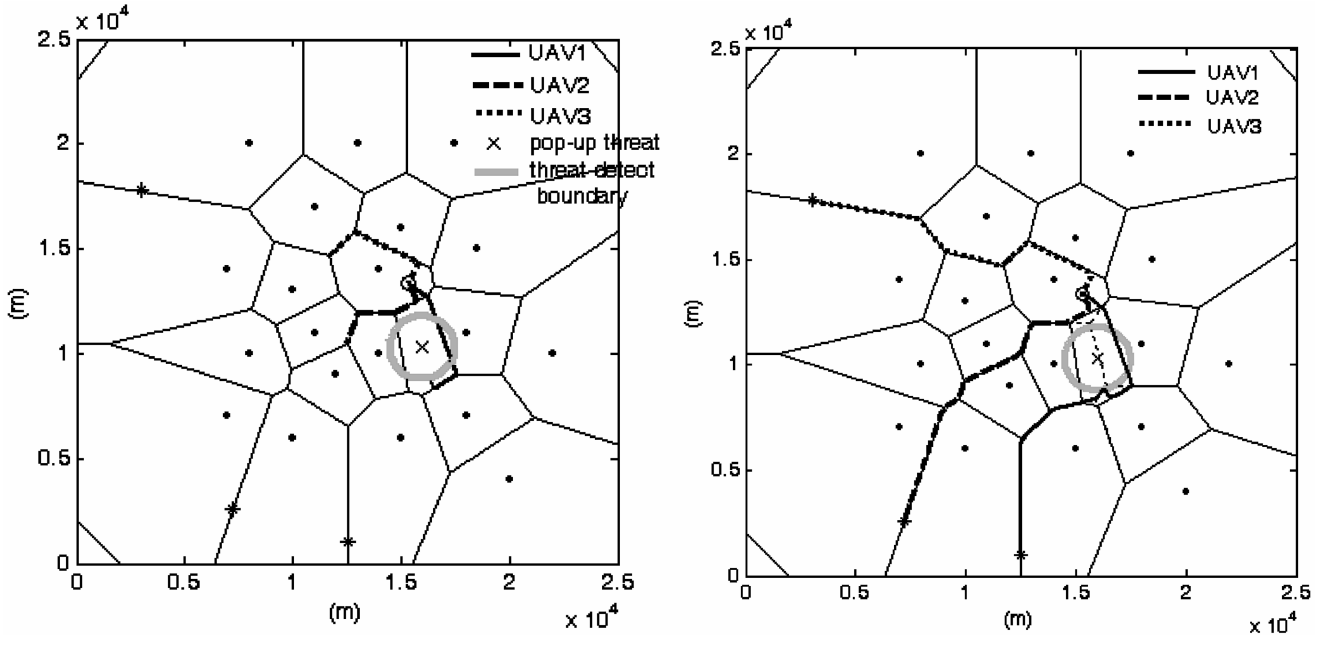

Fig. 10 Replanned path result in the case of a pop-up threat (using the Voronoi diagram). a) Result of replanned path in real time; b) final results in the case of a pop-up threat.

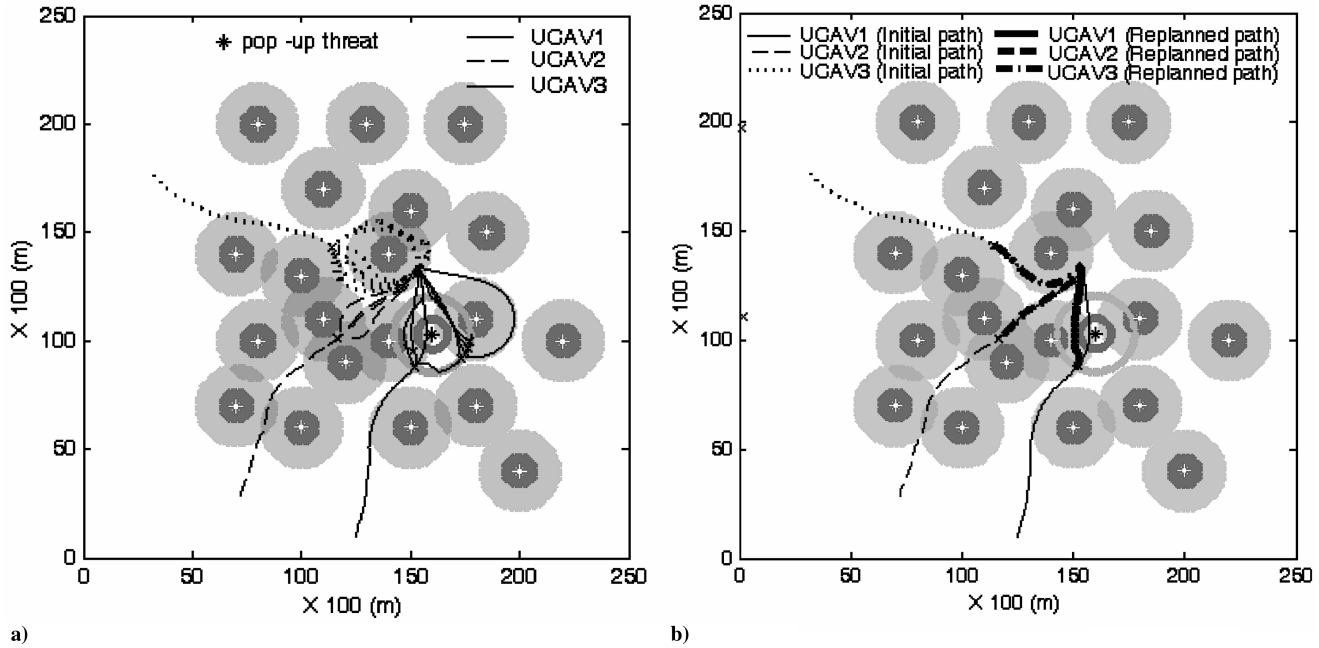

a) b)

Fig. 11 Replanned path result in the case of a pop-up threat (using the potential field method). a) Candidate paths against the pop-up threat; b) final results in the case of a pop-up threat.

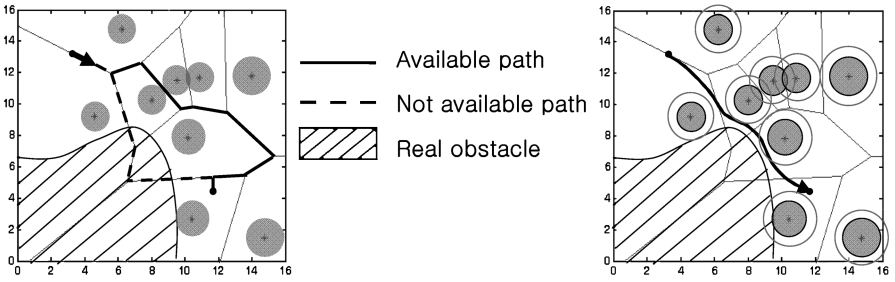

a) b)

Fig. 12 Shortest paths in the case of the existence of a real obstacle.

can reduce the total cost in general situations. Hence the new approach can reduce the total cost as well.

2) The path generated by the new method is continuous and smooth. Thus, if a real-time trajectory is generated, the computed control input may not violate the input magnitude constraint, and the off-tracking error is reduced. But the paths developed by the Voronoi-diagram method consist of straight lines, so that the input magnitude constraint can be easily violated with a large off-tracking error result.

3) Because the diffusion equation holds in $\mathbf{R}^n$, in general, the new approach based upon the diffusion equation can be applied to three-dimensional cases easily. The Voronoi diagram also can be generated in $\mathbf{R}^n$, but application to path planning in $\mathbf{R}^n (n > 2)$ is not straightforward. Path planning using the Voronoi-diagram approach in the 2-D plane except for the rendezvous mission seems to be rather simple and obvious, but in 3-D space the problem becomes quite involved. The Voronoi-diagram method in 3-D space consists of convex polyhedrons, as one path-planning approach between convex polyhedrons is addressed in [16].

4) With real obstacles such as mountains and buildings in battlefields, the new method can easily find appropriate paths by including the boundary conditions of the real obstacles in the potential field computation. But for the Voronoi-diagram method, the nodes and/or edges overlapped with real obstacles are to be excluded in the path planning, or the edges should be modified as shown in Fig. 12a. In such a case, the shortest path is not available due to the real obstacles. Path planning using the Voronoi diagram under real obstacles is investigated in [17], but it is also complicated to produce practical solutions. But in the same situation, the new method can find the best path rather easily as in Fig. 12b.

5) Let us assume that more than one radar exists close to each other. In the Voronoi-diagram method, the path denoted by a bold line in Fig. 13a could be a candidate path although it looks highly risky to pass the space between the two radars. But, for the new method, such a path described in Fig. 13b can never be a candidate path.

On the other hand, there are some disadvantages of the new approach such as the following:

1) Heavy computational time is required to obtain a numerical solution. But, because this computation is executed offline, it does not significantly deteriorate the inherent advantages of the new method.

2) The new algorithm does not generate various candidate paths. The phase of the potential field used in this study is similar to the harmonic function as Fig. 14a. It is not feasible to create a candidate path such as the dashed line in Fig. 14b. But, with the Voronoi diagram it enables us to produce a candidate path represented by the solid line in Fig. 14b. The new method allows us to general multiple paths in general, and it sometimes helps to satisfy the TOT matching condition, but not always. These characteristics could be understood through the TOT versus cost graph.

In Fig. 15, the solid line represents an ideal TOT distribution for the TOT* matching. It is continuous and spread over a wide range. The dashed line, the TOT distribution by the new method is

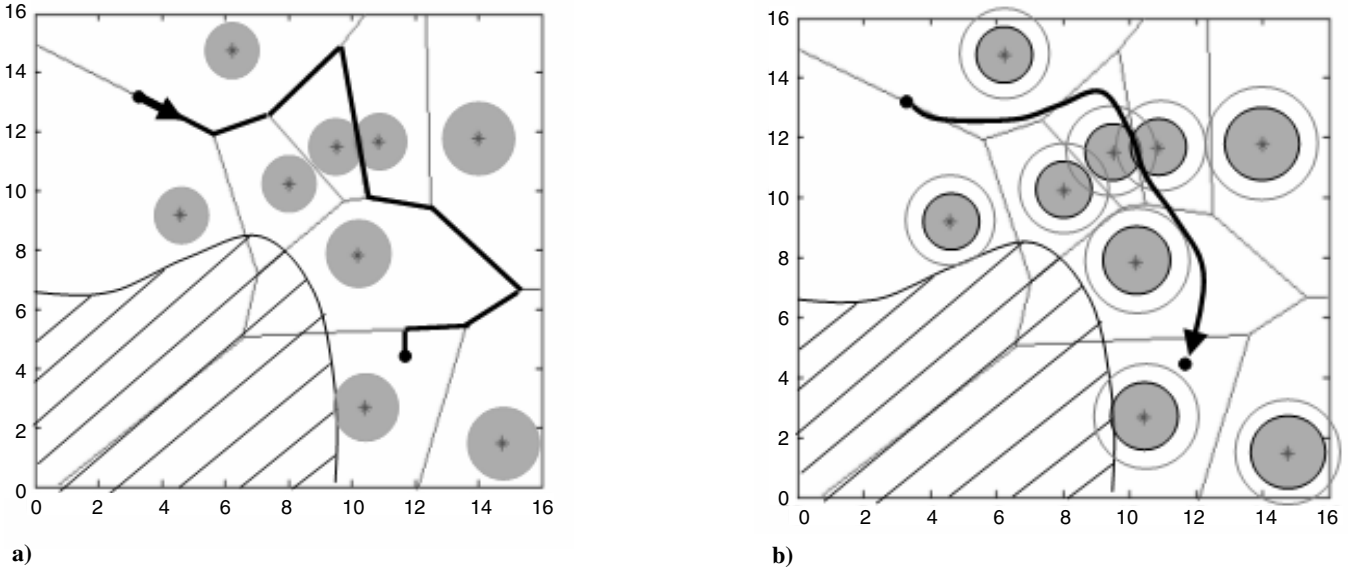

Fig. 13 Candidate paths in the case of very close threats.

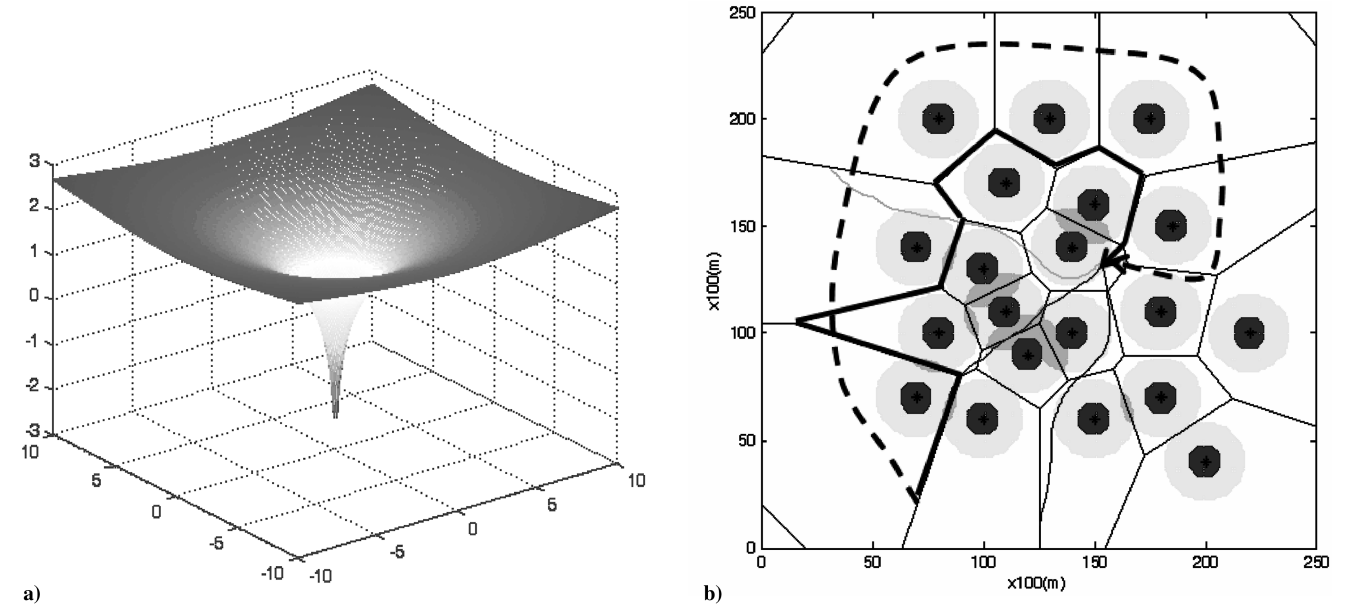

Fig. 14 Variety of candidate paths. a) Phase of potential field; b) an impossible path in the new method and a possible path in the conventional method.

continuous also, but a large range of TOT does not exist. The dotted line, the TOT distribution by the Voronoi diagram, is discontinuous, but large TOT exists. The new potential field-based technique is, therefore, subject to both advantages and disadvantages in terms of the TOT distribution.

3) Sometimes, each path from different UAVs can be overlapped in a close position to the target. Then it is not possible to attack from all different directions, and one needs control laws to establish the final attack angles. A strategy for the attack from different directions has to produce a feasible trajectory over the attack area. The attack area implies the detectable area of anti-aircraft measures at the target location. In this study, the path planning is accomplished in a two-dimensional space. Because UAVs are not a free-flying vehicle, steering and associated control strategies are required. For instance, the exponential control law for mobile robots proposed in [18] could be a solution to this problem.

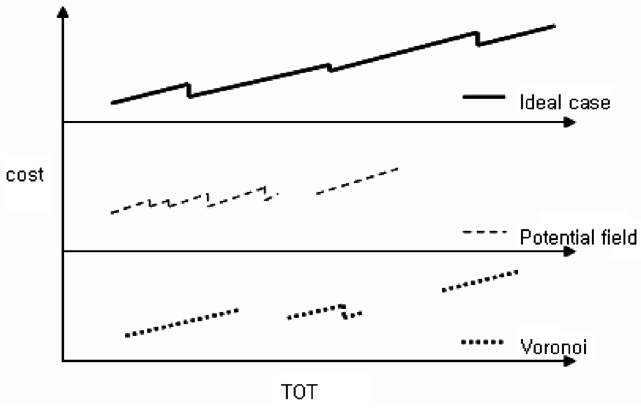

Fig. 15 An example of a TOT distribution for one UAV.

V. Conclusions

As a typical example of the cooperative control for multiple UAVs, an attractive control technique for a SEAD mission is studied. The new strategy is based upon the principle of the potential field theory to cover artificial battlefields. The finite difference numerical solution technique led to multiple candidate paths for the SEAD mission. A continuous and smooth trajectory generation was achieved due to the characteristics of the potential field with sources at the departure points. Various boundary conditions in the numeral solution were used to account for practical obstacles such as enemy radars. Performance of the new approach is compared with the previous approaches by simulation results under the same condition for multiple UAVs departing from all different positions to arrive at the target position simultaneously. It was shown that the total cost decreases by the new method in the simulation results. Moreover, the proposed algorithm is more useful when the path planning in the three-dimensional space is required or real obstacles such as mountains and buildings exist in the battlefield.

Acknowledgment

This research was supported by the Korea Airspace Research Institute (KARI) for a program of development of the CNS/ATM system for the next generation. We truly appreciate their financial support.

References

[1] Beard, R. W., McLain, T. W., and Goodrich, M., "Coordinated Target Assignment and Intercept for Unmanned Air Vehicles," *IEEE International Conference on Robotics and Autonomous*, IEEE, Washington, D.C., May 2002.

[2] McLain, T. W., and Beard, R. W., "Trajectory Planning for Coordinated Rendezvous of Unmanned Air Vehicles," *AIAA Guidance, Navigation, and Control Conference and Exhibit*, AIAA, Denver, CO, Aug. 2000.

[3] Chandler, R. R., and Rasmussen, S., "UAV Cooperative Path Planning," *AIAA Guidance, Navigation, and Control Conference and Exhibit*, AIAA, Denver, CO, Aug. 2000.

[4] McLain, T. W., Chandler, P. R., Rasmussen, S., and Pachter, M., "Cooperative Control of UAV Rendezvous," *American Control Conference*, American Automatic Control Council, Evanston, IL, June 2001.

[5] McLain, T. W., and Beard, R. W., "Coordination Variables, Coordination Functions, and Cooperative-Timing Missions," *Journal of Guidance, Control, and Dynamics*, Vol. 28, No. 1, 2005, pp. 150–161.

[6] Eppstein, D., "Finding the K Shortest Paths," *Society for Industrial and Applied Mathematics Journal of Computations*, Vol. 28, No. 2, 1998, pp. 652–673.

[7] Fox, B. L., "K—The Shortest Paths and Applications to the Probabilistic Networks," *ORSA/TIMS Joint National Meeting*, Las Vegas, Vol. 23, 1975.

[8] Iyengar, S. S., Jorgensen, C. C., Rao, S. V. N., and Weisbin, C. R., "Robot Navigation Algorithm using Learned Spatial Graphs," *Robotica*, Vol. 4, No. 2, 1986, pp. 93–100.

[9] Ramirez, G., and Zeghloul, S., "Collision-Free Path Planning for Nonholonomic Mobile Robots Using a New Obstacle Representation in the Velocity Space," *Robotica*, Vol. 19, No. 5, 2001, pp. 543–555.

[10] Khatib, O., "Real-Time Obstacle Avoidance for Manipulators and Mobile Robots," *International Journal of Robotics Research*, Vol. 5, No. 1, 1986, pp. 90–98.

[11] Schmidt, G. K., and Azarm, K., "Mobile Robot Navigation in a Dynamic World Using an Unsteady Diffusion Equation Strategy," *Proceedings of the IEEE/RSJ International Conference on Intelligent Robots and Systems*, IEEE, Piscataway, NJ, July 1992.

[12] Novy, M. C., "Air Vehicle Optimal Trajectory Between Two Radars," *American Control Conference*, American Automatic Control Council, Evanston, IL, May 2002.

[13] Bortoff, S. A., " Path Planning for UAVs," *Proceedings of the American Control Conference*, American Automatic Control Council, Evanston, IL, June 2000.

[14] Van Nieuwstadt, M. J., and Murray, R. M., "Real-Time Trajectory Generation for Differentially Flat Systems," *International Journal of Robust and Nonlinear Control*, Vol. 8, No. 11, Sept. 1998, pp. 995–1020.

[15] Cormen, T. H., Leiserson, C. E., and Rivest, R. L., *Introduction to Algorithms*, The MIT Press, Cambridge, MA, 1990.

[16] Aronov, B., and Sharir, M., "On Translational Motion Planning of a Convex Polyhedron in 3-Space," *SIAM Journal of Computation*, Vol. 26, No. 6, 1997, pp. 1785–1803.

[17] Agarwal, A., Meng-Hoit, L., and Joo, E. M., "A VoMVi Complex for Supporting Optimal Path Queries for UAVs," *The 2nd International Symposium on Voronoi Diagrams in Science and Engineering*, Seoul, Korea, 2005.

[18] Sordalen, O. J., and Canudas de Wit, C., "Exponential Control Law for a Mobile Robot: Extension to Path Following," *IEEE International Conference on Robotics and Automation*, IEEE, Piscataway, NJ, May 1992.